STUB1 is an intracellular checkpoint for interferon gamma sensing

Simon Ng[1], Shuhui Lim[1], Adrian Chong Nyi Sim[1], Ruban Mangadu[2], Ally Lau[3], Chunsheng Zhang[4], Arun Chandramohan[1], U-Ming Lim[3], Samantha Shu Wen Ho[5], Shih Chieh Chang[1], Pooja Gopal[1], Lewis Z. Hong[5], Andrey Loboda[4], Aaron Zefrin Fernandis[3], Uyen Phan[2], Brian Henry[1], Anthony W. Partridge[1,*]

[1]Quantitative Biosciences, MSD, Singapore

[2]Discovery Oncology, Merck & Co., Inc., South San Francisco, CA, USA

[3]Target & Pathway Biology, MSD, Singapore

[4]Informatics, Merck & Co., Inc., Boston, MA, USA

[5]Translational Biomarkers, MSD, Singapore

*Corresponding author: Anthony W. Partridge (anthony_partridge@merck.com)

Abstract

Immune checkpoint blockade (ICB) leads to durable and complete tumour regression in some patients but in others gives temporary, partial or no response. Accordingly, significant efforts are underway to identify tumour-intrinsic mechanisms underlying ICB resistance. Results from a published mouse model CRISPR screen suggested that targeting an E3 ligase (STUB1) involved with protein homeostasis, may overcome ICB resistance but the molecular basis behind this observation is unclear. Using the ICB-resistant and poorly immunogenic B16-F10 murine melanoma model, we reveal an under-appreciated role of STUB1 to dampen the interferon gamma (IFNγ) response. Deletion of *Stub1* in tumour cells increased IFNGR1 abundance on cellular surface, thus lowering the stimulating threshold of IFNγ. These outcomes translated to IFNγ-enhanced antigen presentation and upregulation of the immunoproteasome complexes. Through proteomics and gene expression profiling, we confirmed STUB1 as a negative regulator of the IFNγ signaling pathway. To block the function of STUB1 in tumour cells, we stably expressed a rationally designed inhibitory biologic, which recapitulated the *Stub1*-null phenotypes in both murine and human tumour cells. Overall, our findings elucidate STUB1 as a barrier for IFNγ sensing and offer a roadmap to pursue STUB1 inhibitors, which may improve tumour response to checkpoint inhibitory therapy.

Introduction

Immune checkpoint blockade (ICB) unleashes the adaptive immune system to fight cancer and results in long-term patient survival unmatched by other drug treatments. Substantial evidence has highlighted IFNγ response and antigen presentation as key components for cancer immunosurveillance and immunotherapy[1-11]. As an emerging paradigm[1,12-14], intact IFNγ sensing in tumours leads to adequate antigen presentation and T cell recognition, but also upregulates PD-L1 to confer immunoevasion[15,16]. Blockade of PD-1/PD-L1 in these patients reinvigorated anti-tumour activity of exhausted T cells and resulted in durable tumour regression[17-19]. In contrast, patients with poor anti-PD-1 response generally have low tumour-infiltrating lymphocytes, low expression of PD-L1 and reduced antigen presentation[20-22]. These ICB-resistant tumours have either preexisting, or post-treatment acquired resistance caused by defective interferon signaling[4,5,23], reduced sensitivity to IFNγ[4,21,24,25], or attenuated antigen presentation not explained by disruptive pathway mutations[22,26-30]. In these circumstances, treating IFNγ-insensitive tumours with ICB is ineffective, thus demanding different approaches or a combination with ICB.

Multiple groups have employed genetic loss-of-function screens to identify targets that underly ICB resistance or the targets required for anti-tumour immunity. By mining the repository of CRISPR screens (BioGRID ORCS)[31], we noted that loss of *Stub1* appears to reverse the resistance of immunotherapy in an *in vivo* tumour mouse model[9] and enhance T cell-mediated killing of *in vitro* murine tumour cells (B16-F10[10], CT26[32] and Renca[32]). As well, low STUB1 correlates with high PD-L1 in human HAP1 and A375 cells[33]. Although the underlying mechanisms remain elusive, recurring discovery of STUB1 among the top 1% hits in these genetic screens, as summarized in Supplementary Table 1, highlight a significant, yet under-

appreciated role of STUB1 in regulating anti-tumour immunity. Based on the unbiased screening results and the canonical role of STUB1 in response to stress stimuli[34-36], we hypothesize that STUB1 may play a conserved and prominent part in dampening stress triggered by the immune system.

To study the molecular role of *Stub1*, we used CRISPR-editing to delete *Stub1* from an ICB-resistant and poorly immunogenic[37] murine melanoma line (B16-F10) by electroporating the corresponding crRNA/tracrRNA/Cas9 ribonucleoprotein into these cells. We isolated a total of nine *Stub1*-null cells by single-cell subcloning (Supplementary Table 2). For most experiments, we focused on two clonal cell lines – gStub1 #1 (1D10) and gStub1 #2 (1A12) – targeted by two independent crRNA respectively.

Stub1 deficiency enhances antigen presentation *via* increased IFNγ responsiveness

Tumours frequently reduce antigen presentation to evade immunosurveillance and immunotherapy[5,22,27,38]. Accordingly, we measured the effect of *Stub1* deletion on major histocompatibility complex class I (MHC-I) surface expression in B16-F10 cells by flow cytometry. Strikingly, relative to parental and control cells, tumour cells lacking *Stub1* displayed significantly higher, IFNγ-dependent, MHC-I on cell surface (Fig. 1a). The differential antigen presentation is consistently found across all nine *Stub1*-null cells isolated *via* single-cell subcloning (Supplementary Fig. 1a–e and Supplementary Table 2). We regularly observed differential expression of MHC-I at different doses of IFNγ (Fig. 1b–c and Supplementary Fig. 1f). The IFNγ-STAT1-IRF1 axis induces genes associated with antigen processing and presentation. Remarkably, *Stub1* deletion led to upregulation of STAT1, STAT2, and IRF1 after 24 h stimulation with IFNγ (Fig. 1d). Immunoproteasome complex has been associated with better tumour immunogenicity and better prognosis and response to checkpoint therapies in melanoma[39]. Similarly, in an IFNγ-dependent manner, *Stub1* deletion upregulated PSMB8, PSMB9 and PSMB10, which are the subunit of the immunoproteasome complexes (Fig. 1d–e). The differential protein expression of STAT1, STAT2, IRF1, PSMB9 and PSMB10 are maintained across all doses of IFNγ, whereas PSMB8 upregulation is more pronounced at doses higher than 0.30 ng ml^{-1} (Fig. 1e and Supplementary Fig. 1g–h). To measure the initial response of the signal transduction, we treated the tumour cells with a titration of IFNγ and harvested the cellular lysates for analysis at 2 h post-stimulation. Loss of *Stub1* substantially lowers the stimulating threshold of IFNγ required for the early induction of IRF1 and the phosphorylation of Tyr701-STAT1 (Fig. 1f). Total STAT1 protein level remains low and stable during the early response (Fig. 1f) but was significantly upregulated at 24 h post-stimulation (Fig. 1d). Overall, parental B16-F10 and control cells demanded at least 10-fold higher concentration of IFNγ to achieve a comparable response observed in *Stub1*-null cells (Fig. 1b and 1e), suggesting *Stub1* is a key checkpoint for IFNγ sensing in tumour cells.

Stub1 constrains IFNγ response by downregulating IFNγ receptors

To investigate how *Stub1* constitutively suppresses the IFNγ response, we turned to the level of IFNγ receptor 1 (IFNGR1) in B16-F10 cells (Fig. 2a). Indeed, loss of *Stub1* increased the surface

expression level of IFNGR1 under both resting and IFNγ-stimulating conditions (Fig. 2b–c and Supplementary Fig. 2a). Interestingly, the cell surface level of IFNGR1 declined with increasing IFNγ concentration (Fig. 2b), perhaps through feedback endocytosis of the ligand-receptor complexes[40]. The regulation is specific as *Stub1* deletion has no significant effects for other cytokine receptors, such as IL1R1, IL6R, GP130 and IFNAR1 (Fig. 2d, Supplementary Fig. 2b–c). Stable gene expression of *Ifngr1* suggested that downregulation of the receptor by the E3 ligase STUB1 occurs at the protein level (Supplementary Fig. 2d).

We reasoned that IFNGR1, being constitutively upregulated in *Stub1*-null cells, could potentiate and amplify the downstream signal transduction. To broadly evaluate the response, we studied the gene expression of 750 immune-related genes (NanoString PanCancer IO 360; Supplementary Table 3). Overall, most genes have comparable expression among the *Stub1*-null and control cells (Supplementary Fig. 3a). As expected, *Stub1*-null cells had an enhanced response to IFNγ treatment (6 h or 24 h) as evidence by the increased induction of interferon-stimulated genes (ISGs), including those that govern the interferon signaling pathway (*Stat1*, *Stat2*, *Irf1* and *Irf9*), antigen processing and presentation (*H2-D1*, *H2-K1*, *B2m*, *Nlrc5*, *Tap1*, *Tapbp*, *Tapbpl*, *Psmb9* and *Psmb10*), and chemotaxis of immune cells (*Cxcl10* and *Csf1*) (Fig. 2e, Supplementary Fig. 3b–c). In contrast, the control cells weakly induced these ISGs, in response to IFNγ stimulation for 6 h, and the ISGs mostly receded at 24 h post-stimulation (Fig. 2e, Supplementary Fig. 3d). Importantly, *Stub1* does not directly regulate the ISGs themselves, as evidenced by their comparable gene expression (Fig. 2e and Supplementary Fig. 2d) and protein levels (Fig. 1d–f) among the untreated *Stub1*-null and control cells.

To investigate IFNγ signaling at the protein level, we performed proteome-wide analysis with mass spectrometry (MS). A high-quality dataset consisting of ~2300 proteins (Supplementary Table 4) definitively validated our hypothesis – STUB1 is a checkpoint and barrier for IFNγ sensing. Loss of STUB1 sensitized tumour cells to IFNγ exposure and led to statistically significant enrichment of the protein targets of ISGs, including those required for antigen presentation such as H2-K1, B2M, PSME1, PSME2 and ERAP1 (Fig. 2f). Overall, we identified an overlapping set of 13 proteins (explicitly labeled in Fig. 2f), all inducible by interferon, being enriched in both independent *Stub1*-null cells relative to the control cells (Fig. 2g and Supplementary Fig. 3e). Taken together, we propose a framework whereby STUB1 may confer ICB resistance by downregulating IFNGR1 on the cell surface, thus curbing the tumour cells' ability to sense and respond to IFNγ (Fig. 2h).

Inhibition of STUB1 phenocopies the genetic knockout

A recent study[41] identified a high-affinity peptide (SIWWPD) capable of blocking the interaction of STUB1 with HSPA8 – a chaperone bound to STUB1 through its C-terminal peptide. We validated the binding of the inhibitory peptide using multiple orthogonal biophysical assays[42], such as isothermal titration calorimetry (K_D = 14 ± 2 nM, Fig. 3a and Supplementary Fig. 4a–c), thermal shift assay (ΔT_m = 18.3 ± 0.1 °C, Fig. 3b), and fluorescence polarization assay (IC_{50} = 0.34 ± 0.02 μM, Fig. 3c). We also designed a control peptide (SIWWHR), where STUB1 binding is abolished (K_D > 10 μM, IC_{50} > 100 μM, ΔT_m = -0.1 ± 0.2 °C, Fig. 3a–c and

Supplementary Fig. 4c–d) by substituting two key interacting residues (Pro-Asp) with counter-productive ones (His-Arg). To investigate if stoichiometric STUB1 inhibition could recapitulate the *Stub1*-null phenotypes, we engineered B16-F10 cells to constitutively and stably express a fusion protein consisting of an mCherry2 reporter[43] tagged on its C-terminus with the inhibitory peptide or control sequence (Fig. 3d–e). As expected, ectopic expression of mCherry2-SIWWPD, but not its control, led to upregulation of IFNGR1 on the cell surface of B16-F10, under both resting and IFNγ-stimulating conditions (Fig. 3f). Furthermore, this effect was not restricted to murine cells as stable expression of the inhibitory biologic in human tumour cells (A375 and A549) also resulted in the same phenotype (Fig. 3f), which in turn potentiated the cells to boost the surface levels of MHC-I in response to IFNγ (Fig. 3g). Importantly, the interaction between the expressed biologic and STUB1 is specific, as STUB1 was co-precipitated with FLAG-mCherry2-SIWWPD, but not its control, from the cellular lysate (Fig. 3h). The interaction is completely reversible in a dose-dependent manner by spiking synthetic peptide inhibitor into the mixture of co-immunoprecipitation. Overall, stoichiometric inhibition of STUB1 with the expressed biologic successfully recapitulated the phenotypes of *Stub1*-null cells shown earlier (Fig. 1c for MHC-I, and Fig. 2c for IFNGR1), an important result as pharmacological inhibition may not always mimic the outcome of a genetic knockout.

Clinical relevance of *STUB1* across multiple tumours

Previous analysis of data from KEYNOTE clinical trials demonstrated that tumour mutational burden (TMB) and an 18-gene T-cell inflamed, IFNγ-related gene expression profile (GEP) has predictive value in identifying anti-PD-1 responders and non-responders[7,19]. TMB and GEP have low correlation and are tissue-agnostic measures that independently predict anti-PD-1 responsiveness in multiple tumours. Accordingly, we analyzed the correlation of *STUB1* with TMB and GEP using the bulk RNAseq data from The Cancer Genome Atlas (TCGA) dataset. The resulting analysis showed that *STUB1* is slightly depleted in tumours associated with high GEP score (top 55th percentile, GEP^{hi}) regardless of the TMB value (Fig. 4a). To explore the expression level of *STUB1* in different cell types, we deconvoluted the bulk RNAseq data with CIBERSORT analysis[44] in each tumour type from TCGA (Fig. 4b). In general, *STUB1* is relatively low in the immune effector cells, such as activated NK cells, $CD8^+$ T cell, $\gamma\delta^+$ T cell, and activated dendritic cells. Interestingly, *STUB1* expression is higher in M0 and M2 macrophage, relative to M1 macrophage, across the majority of the tumour types. These analyses were repeated using Moffit dataset (Supplementary Fig. 5a, 5b) and the trends are mostly consistent with TCGA dataset (Fig. 4a, 4b). Finally, we compared *STUB1* expression in tumours and adjacent normal tissues across multiple tumour types for which the data are available in TCGA (Fig. 4c). *STUB1* is overexpressed in thyroid, kidney, prostate and breast tumours relative to their adjacent normal tissues, whereas a reverse trend is found in gastric cancer. Overall, the association of underexpression of *STUB1* in an inflamed tumour microenvironment (GEP^{hi}) and the overexpression of *STUB1* in immunologically "cold" tumours (prostate and breast) support our interpretation of *STUB1* as an immunosuppressive gene, which likely constrains IFNγ sensing in the cancer-immunity cycle[45].

Discussion

Emerging evidence[9,10,32,33,46] point to a role for STUB1 in tumour immune evasion and anti-PD-1 resistance. However, the underlying mechanisms have been largely unclear. STUB1 protein[47] is evolutionarily conserved among many species[48]. The protein is highly homologous (>97% identical) between human and mouse, with absolute identity at the chaperone binding pocket. Here, using ICB-resistant murine melanoma model, we provide multiple lines of evidence that ubiquitin ligase STUB1 downregulates IFNGR1 to dampen IFNγ sensing. During preparation of this manuscript, Peeper and co-workers arrived at a similar conclusion where they elegantly identified STUB1 as a pivotal regulator of IFNGR1 through CRISPR screen and further pinpointed the ubiquitination site on IFNGR1 with MS proteomics[49]. This independent finding further strengthens the case of STUB1 as an intracellular checkpoint and barrier for IFNγ sensing. Together, the cumulative evidence nominates STUB1 as a promising immuno-oncology target. Accordingly, it is worth considering the druggability of this target as well as its potential for on-target toxicities, which we elaborate below.

Traditionally, protein-protein interaction (PPI) targets have been challenging to tackle with small molecules due to their large and flat surfaces. Such challenge has prompted researchers to explore alternative approaches. Indeed, the inhibition of STUB1 with mCherry2-peptide fusion, as demonstrated here, suggests that STUB1 could be therapeutically addressed with a peptide-based strategy. For such efforts to advance, proteolytic stability and permeability must be addressed while maintaining drug-like properties. Recent efforts using macrocyclic display technology and/or all-D approaches could be leveraged in that regard[50,51]. On the other hand, E3 ligases may represent a subclass of PPIs which are tractable by small molecules. Successful examples include MDM2, VHL, cIAP, and CRBN, for which small molecules have been identified and extended in PROTAC application.

Although attractive as an immuno-oncology target, inhibition of STUB1 has the potential for on-target toxicity. Accordingly, efforts to gain insights to the therapeutic window are warranted. A progressive neurologic disorder known as SCAR16[52,53] was linked to biallelic loss-of-function (LoF) germline mutations in *STUB1*. Patients with missense mutation in *STUB1* are characterized with substantial loss of purkinje cells[54] in cerebellum which coordinates movement control. Although patients could tolerate LoF mutation in *STUB1*, they display the phenotype of ataxia and aging appearance. Accordingly, it seems important to design *STUB1* inhibitors that do not impact the neural tissues by not crossing the blood-brain barrier. Intriguingly, clinical study reveals that SCAR16 patients surprisingly exhibit a broad spectrum of autoimmune disorders including type I diabetes, alopecia, ulcerative colitis, uveitis and pancreatitis[55]. These observations provide real-world evidence that support STUB1 serving a potential role in keeping the immune system in balance.

In summary, our results highlight STUB1 as an intracellular checkpoint for IFNγ sensing. Loss of *Stub1* increased tumour cells' sensitivity for IFNγ, which in turn upregulated ISGs expression and enhanced antigen processing and presentation *in vitro*. These outcomes are most likely

attributed to the physiological role of STUB1 to constitutively downregulating the surface level of IFNGR1 in tumour cells, thereby reducing their ability to sense IFNγ – a key cytokine secreted by activated T cells and NK cells. Live cell imaging and cellular studies demonstrated that STUB1, as a fusion with EGFP reporter, was released from cytosolic chaperones during acute heat shock or stress caused by HSP70 and HSP90 inhibitors[56]. Once being released, EGFP-STUB1 accumulated at the cellular membrane. This observation provides a plausible mechanism for STUB1 to engage and regulate the IFNγ receptor. Finally, we demonstrated that pharmacological inhibition of STUB1 with ectopic expression of a biologic phenocopied the genetic knockout. Targeting STUB1 may offer a rational approach to improve the anti-tumour immunity when combined with anti-PD-1. Our study provides motivation for the discovery of chemical probes for STUB1. Not only would those prove valuable for interrogating whether the inhibitors would have a therapeutic window but would also serve as potential leads for the development of clinical compounds. If that latter goal could be achieved, a wider range of cancer patients would be predicted to benefit from checkpoint inhibitory therapy.

References

1 Dighe, A. S., Richards, E., Old, L. J. & Schreiber, R. D. Enhanced in vivo growth and resistance to rejection of tumor cells expressing dominant negative IFNγ receptors. *Immunity* **1**, 447-456 (1994).

2 Kaplan, D. H. *et al.* Demonstration of an interferon γ-dependent tumor surveillance system in immunocompetent mice. *Proc. Natl. Acad. Sci. U. S. A.* **95**, 7556-7561 (1998).

3 Shankaran, V. *et al.* IFNγ and lymphocytes prevent primary tumour development and shape tumour immunogenicity. *Nature* **410**, 1107-1111 (2001).

4 Gao, J. *et al.* Loss of IFN-γ Pathway Genes in Tumor Cells as a Mechanism of Resistance to Anti-CTLA-4 Therapy. *Cell* **167**, 397-404.e399 (2016).

5 Zaretsky, J. M. *et al.* Mutations Associated with Acquired Resistance to PD-1 Blockade in Melanoma. *New Engl. J. Med.* **375**, 819-829 (2016).

6 Patel, S. J. *et al.* Identification of essential genes for cancer immunotherapy. *Nature* **548**, 537-542 (2017).

7 Ayers, M. *et al.* IFN-γ–related mRNA profile predicts clinical response to PD-1 blockade. *The Journal of Clinical Investigation* **127**, 2930-2940 (2017).

8 Jerby-Arnon, L. *et al.* A Cancer Cell Program Promotes T Cell Exclusion and Resistance to Checkpoint Blockade. *Cell* **175**, 984-997.e924 (2018).

9 Manguso, R. T. *et al.* In vivo CRISPR screening identifies Ptpn2 as a cancer immunotherapy target. *Nature* **547**, 413-418 (2017).

10 Pan, D. *et al.* A major chromatin regulator determines resistance of tumor cells to T cell–mediated killing. *Science* **359**, 770 (2018).

11 Kearney, C. J. *et al.* Tumor immune evasion arises through loss of TNF sensitivity. *Science Immunology* **3**, eaar3451 (2018).

12 Alspach, E., Lussier, D. M. & Schreiber, R. D. Interferon γ and Its Important Roles in Promoting and Inhibiting Spontaneous and Therapeutic Cancer Immunity. *Cold Spring Harb. Perspect. Biol.* **11** (2019).

13 Kalbasi, A. & Ribas, A. Tumour-intrinsic resistance to immune checkpoint blockade. *Nature Reviews Immunology* **20**, 25-39 (2020).

14 Grasso, C. S. *et al.* Conserved Interferon-γ Signaling Drives Clinical Response to Immune Checkpoint Blockade Therapy in Melanoma. *Cancer Cell* (2020).

15 Garcia-Diaz, A. *et al.* Interferon Receptor Signaling Pathways Regulating PD-L1 and PD-L2 Expression. *Cell Rep.* **19**, 1189-1201 (2017).

16 Benci, J. L. *et al.* Tumor Interferon Signaling Regulates a Multigenic Resistance Program to Immune Checkpoint Blockade. *Cell* **167**, 1540-1554.e1512 (2016).

17 Eroglu, Z. *et al.* High response rate to PD-1 blockade in desmoplastic melanomas. *Nature* **553**, 347-350 (2018).

18 Tumeh, P. C. *et al.* PD-1 blockade induces responses by inhibiting adaptive immune resistance. *Nature* **515**, 568-571 (2014).

19 Cristescu, R. *et al.* Pan-tumor genomic biomarkers for PD-1 checkpoint blockade–based immunotherapy. *Science* **362**, eaar3593 (2018).

20 Herbst, R. S. *et al.* Predictive correlates of response to the anti-PD-L1 antibody MPDL3280A in cancer patients. *Nature* **515**, 563-567 (2014).

21 Chen, P.-L. *et al.* Analysis of Immune Signatures in Longitudinal Tumor Samples Yields Insight into Biomarkers of Response and Mechanisms of Resistance to Immune Checkpoint Blockade. *Cancer Discov.* **6**, 827 (2016).

22 Rodig, S. J. *et al.* MHC proteins confer differential sensitivity to CTLA-4 and PD-1 blockade in untreated metastatic melanoma. *Sci. Transl. Med.* **10**, eaar3342 (2018).
23 Sucker, A. *et al.* Acquired IFNγ resistance impairs anti-tumor immunity and gives rise to T-cell-resistant melanoma lesions. *Nat. Commun.* **8**, 15440 (2017).
24 Klampfer, L. *et al.* Oncogenic Ki-Ras Inhibits the Expression of Interferon-responsive Genes through Inhibition of STAT1 and STAT2 Expression. *J. Biol. Chem.* **278**, 46278-46287 (2003).
25 Chandrasekaran, S. *et al.* Phosphoinositide 3-Kinase Signaling Can Modulate MHC Class I and II Expression. *Mol. Cancer Res.* **17**, 2395 (2019).
26 Yamamoto, K. *et al.* Autophagy promotes immune evasion of pancreatic cancer by degrading MHC-I. *Nature* (2020).
27 Garrido, F., Aptsiauri, N., Doorduijn, E. M., Garcia Lora, A. M. & van Hall, T. The urgent need to recover MHC class I in cancers for effective immunotherapy. *Curr. Opin. Immunol.* **39**, 44-51 (2016).
28 Perea, F. *et al.* The absence of HLA class I expression in non-small cell lung cancer correlates with the tumor tissue structure and the pattern of T cell infiltration. *Int. J. Cancer* **140**, 888-899 (2017).
29 Gettinger, S. *et al.* Impaired HLA Class I Antigen Processing and Presentation as a Mechanism of Acquired Resistance to Immune Checkpoint Inhibitors in Lung Cancer. *Cancer Discov.* **7**, 1420 (2017).
30 Lee, J. H. *et al.* Transcriptional downregulation of MHC class I and melanoma de- differentiation in resistance to PD-1 inhibition. *Nat. Commun.* **11**, 1897 (2020).
31 Oughtred, R. *et al.* The BioGRID interaction database: 2019 update. *Nucleic Acids Res.* **47**, D529-D541 (2019).
32 Lawson, K. A. *et al.* Functional genomic landscape of cancer-intrinsic evasion of killing by T cells. *Nature* **586**, 120-126 (2020).
33 Mezzadra, R. *et al.* Identification of CMTM6 and CMTM4 as PD-L1 protein regulators. *Nature* **549**, 106-110 (2017).
34 Jiang, J. *et al.* CHIP Is a U-box-dependent E3 Ubiquitin Ligase. *J. Biol. Chem.* **276**, 42938-42944 (2001).
35 Murata, S., Minami, Y., Minami, M., Chiba, T. & Tanaka, K. CHIP is a chaperone-dependent E3 ligase that ubiquitylates unfolded protein. *EMBO reports* **2**, 1133-1138 (2001).
36 Qian, S.-B., McDonough, H., Boellmann, F., Cyr, D. M. & Patterson, C. CHIP-mediated stress recovery by sequential ubiquitination of substrates and Hsp70. *Nature* **440**, 551-555 (2006).
37 Mosely, S. I. S. *et al.* Rational Selection of Syngeneic Preclinical Tumor Models for Immunotherapeutic Drug Discovery. *Cancer Immunology Research* **5**, 29 (2017).
38 Sade-Feldman, M. *et al.* Resistance to checkpoint blockade therapy through inactivation of antigen presentation. *Nat. Commun.* **8**, 1136 (2017).
39 Kalaora, S. *et al.* Immunoproteasome expression is associated with better prognosis and response to checkpoint therapies in melanoma. *Nat. Commun.* **11**, 896 (2020).
40 Farrar, M. A., Fernandez-Luna, J. & Schreiber, R. D. Identification of two regions within the cytoplasmic domain of the human interferon-gamma receptor required for function. *J. Biol. Chem.* **266**, 19626-19635 (1991).
41 Ravalin, M. *et al.* Specificity for latent C termini links the E3 ubiquitin ligase CHIP to caspases. *Nat. Chem. Biol.* **15**, 786-794 (2019).
42 Ng, S. *et al.* De-risking Drug Discovery of Intracellular Targeting Peptides: Screening Strategies to Eliminate False-Positive Hits. *ACS Med. Chem. Lett.* **11**, 1993-2001 (2020).
43 Shen, Y., Chen, Y., Wu, J., Shaner, N. C. & Campbell, R. E. Engineering of mCherry variants with long Stokes shift, red-shifted fluorescence, and low cytotoxicity. *PLoS One* **12**, e0171257 (2017).

44 Newman, A. M. *et al.* Robust enumeration of cell subsets from tissue expression profiles. *Nat. Methods* **12**, 453-457 (2015).

45 Chen, Daniel S. & Mellman, I. Oncology Meets Immunology: The Cancer-Immunity Cycle. *Immunity* **39**, 1-10 (2013).

46 Zhou, P. *et al.* MLL5 suppresses antiviral innate immune response by facilitating STUB1-mediated RIG-I degradation. *Nat. Commun.* **9**, 1243 (2018).

47 Ballinger, C. A. *et al.* Identification of CHIP, a Novel Tetratricopeptide Repeat-Containing Protein That Interacts with Heat Shock Proteins and Negatively Regulates Chaperone Functions. *Mol. Cell. Biol.* **19**, 4535 (1999).

48 Zhang, M. *et al.* Chaperoned Ubiquitylation–Crystal Structures of the CHIP U Box E3 Ubiquitin Ligase and a CHIP-Ubc13-Uev1a Complex. *Mol. Cell* **20**, 525-538 (2005).

49 Apriamashvili, G. *et al.* Loss of Ubiquitin Ligase STUB1 Amplifies IFNγ-R1/JAK1 Signaling and Sensitizes Tumors to IFNγ. 2020.2007.2007.191650 (2020).

50 Kannan, S. *et al.* Macrocyclization of an all-d linear α-helical peptide imparts cellular permeability. *Chemical Science* **11**, 5577-5591 (2020).

51 Vinogradov, A. A., Yin, Y. & Suga, H. Macrocyclic Peptides as Drug Candidates: Recent Progress and Remaining Challenges. *J. Am. Chem. Soc.* **141**, 4167-4181 (2019).

52 Shi, Y. *et al.* Identification of CHIP as a Novel Causative Gene for Autosomal Recessive Cerebellar Ataxia. *PLoS One* **8**, e81884 (2013).

53 Ronnebaum, S. M., Patterson, C. & Schisler, J. C. Emerging evidence of coding mutations in the ubiquitin–proteasome system associated with cerebellar ataxias. *Human Genome Variation* **1**, 14018 (2014).

54 Chen, D.-H. *et al.* Heterozygous *STUB1* missense variants cause ataxia, cognitive decline, and STUB1 mislocalization. *Neurology Genetics* **6**, e397 (2020).

55 Heimdal, K. *et al.* STUB1 mutations in autosomal recessive ataxias – evidence for mutation-specific clinical heterogeneity. *Orphanet J. Rare Dis.* **9**, 146 (2014).

56 Kopp, Y. *et al.* CHIP as a membrane-shuttling proteostasis sensor. *eLife* **6**, e29388 (2017).

57 Panda, A. *et al.* Identifying a Clinically Applicable Mutational Burden Threshold as a Potential Biomarker of Response to Immune Checkpoint Therapy in Solid Tumors. *JCO Precision Oncology*, 1-13 (2017).

Acknowledgements

We thank MSD for the financial support. SN acknowledges support from the MRL Postdoctoral Research Program.

Competing interests

All authors are current employees of subsidiaries of Merck & Co., Inc., Kenilworth, NJ, USA

Methods

Protein and peptides

Recombinant STUB1 protein, spanning aa25-aa153, was produced by Nanyang Technological University protein production platform. The purity and identity of the protein was confirmed by mass spectrometry and SDS-PAGE. Synthetic peptides, in a form of N-acetylation and free C-terminal carboxylic acid, were custom made by Chinese Peptide Company (CPC). The purity and identity of the peptides were confirmed by analytic HPLC (≥95% purity) and mass spectrometry. Peptides are dissolved in neat DMSO as 10 mM stock solution and diluted thereof for subsequent experiments.

Cell lines and culture

Murine melanoma B16-F10 (CRL-6475), human melanoma A375 (CRL-1619) and human lung A549 (CCL-185) were purchased from ATCC. Parental and engineered B16-F10 or A375 were cultured in DMEM (Gibco, #10569010) supplemented with 10% FBS (HyClone, #SH30071.03). Parental and engineered A549 cells were cultured in Ham's F-12K (Gibco, #21127022) supplemented with 10% FBS (HyClone, #SH30071.03). All cells were maintained at 37 °C, 5% CO_2, and 95% relative humidity. The cells were routinely tested for mycoplasma. The CRISPR-engineered cell lines were PCR-evaluated by IDEXX BioAnalytics to be free of viral contamination, were genetically confirmed as mouse origin, and had almost identical short tandem repeat profile (>90% match) to that established for B16-F10 (ATCC, CRL-6475). Cell number was determined using NC-100 NucleoCounter (ChemoMetec).

Generation of CRIPSR-edited tumour cell lines

B16-F10 cells were genetically edited by electroporating the Cas9/crRNA/tracrRNA ribonucleoprotein (RNP) complexes into cells using the 4D-nucleofector system (Lonza). To prepare the guide RNA complex, a 1:1 mixture of Alt-R® crRNA and tracrRNA (50 μM each, IDT) in nuclease-free duplex buffer (IDT) was heated at 95 °C for 5 min, followed by cooling to room temperature. The annealed guide RNA complex (150 pmol) was subsequently mixed with Alt-R® S.p. HiFi Cas9 Nuclease V3 (100 pmol, IDT, #1081060), and the resulting mixture was incubated at room temperature for 10 min to form the final RNP complexes. B16-F10 cells (2×10^5) were rinsed with PBS and re-suspended in 20 μl SF nucleofactor solution (Lonza, V4XC-2032), followed by combining with the RNP complexes (4.6 μl). The resulting cell suspension was transferred to a designated well of nucleocuvette strip which was then pulsed with the nucleofector system using DJ-110 preset. After pulsing, culture media (75 μl) was added and the cell suspension was transferred to a designated well of a 12-well plate filled with 1.0 ml DMEM + 10% FBS. After 48 h incubation, the CRISPR-edited cells were subcloned by limiting dilution. The monoclonal cell lines were validated by analyzing the Sanger sequencing results of the PCR amplicon (~800 bp) flanking the crRNA-targeted site using ICE v2 CRISPR analysis tool (Synthego). Loss of STUB1 protein was confirmed by Western blot analysis.

Stub1 crRNA1: GCATTGCTAAGAAGAAGCGC;

Stub1 crRNA2: ACTTGCGGCCCACGAAGAGC;

control crRNA: GCGAGGTATTCGGCTCCGCG.

Generation of tumour cell lines expressing mCherry2-peptide fusion

To generate the plasmids, gBlocks® gene fragments (IDT) encoding the inhibitory biologic (FLAG-mCherry2-GGSGGS-SIWWPD) and the control biologic (FLAG-mCherry2-GGSGGS-SIWWHR) were cloned into pEF6 vector (Thermo Fisher Scientific) by standard restriction enzyme digestion and T4 DNA ligation. The final constructs were verified by Sanger sequencing. Coding sequences of the constructs are provided in Supplementary Table 5. To generate the stable cell lines, a total of 2×10^5 B16-F10, A375 or A549 cells were electroporated with 200 ng plasmid using DJ-110, FF-120 or CM-130 respectively – the preset programmed in 4D-nucleofector system (Lonza). The preparation of the cell suspension and the process of the electroporation are similar to that described in the CRISPR method section. The stable cell lines were selected using 10 μg ml^{-1} blasticidin three days post-electroporation and were maintained in 5 μg ml^{-1} blasticidin once the stable colonies were established.

In vitro stimulation with IFNγ

Parental, CRISPR-edited or biologic-overexpressed tumour cells were seeded in a cell density of 60,000 (B16-F10), 100,000 (A375) or 200,000 (A549) per well in 12-well plate filled with 0.8 ml culture media + 10% FBS. After overnight incubation, the culture media were replaced with 1 ml fresh media supplemented with 10% FBS and the designated concentration of the recombinant mouse IFNγ (R&D Systems, #485-MI-100) or recombinant human IFNγ (R&D Systems, #285-IF-100). The cells were stimulated with the cytokine for 24 h before they were harvested by trypsinization for flow cytometry, western blot, or qPCR analysis (6 h treatment).

Flow cytometry analysis

Cells were dissociated from the wells with 0.25% trypsin (Gibco, 25200056). After rinsing with 0.5 ml PBS, each sample was stained with the LIVE/DEAD Fixable Aqua dead cell staining solution (Life Technologies, L34957) in 100 μl PBS (1:1000 dilution) for 15 min at 4 °C. After rinsing with 2 × 0.5 ml PBS, each sample was stained with the corresponding primary antibody-dye conjugates diluted in 100 μl Pharmingen stain buffer (BD Biosciences, #554657). After 1 h staining at 4 °C, the cells were rinsed with 2 × 2 ml Pharmingen stain buffer and fixed with 4.21% (w/w) formaldehyde (BD Biosciences, #554655). Samples were analyzed on LSRFortessa X-20 (BD Biosciences) with appropiate fluorescence compensation. Primary antibodies used were: H-$2K^b$/H-$2D^b$ (FITC, Biolegend, #114606, 1:50 dilution), HLA-A,B,C (FITC, Biolegend, #311404, 1:100 dilution), mouse IFNGR1 (PE, Invitrogen, #12-1191-82, 1:50 dilution), human IFNGR1 (PE, Biolegend, # 308704, 1:50 dilution), mouse IL1R1 (APC, Biolegend, #113509, 1:20 dilution), mouse IL6R (APC, Biolegend, #115812, 1:20 dilution), mouse IFNAR1 (APC, Biolegend, #127314, 1:20 dilution), and mouse GP130 (PE, Biolegend, #149404, 1:100 dilution).

Western blot analysis

Cells were dissociated from the wells with 0.25% trypsin (Gibco, 25200056). After rinsing with 0.5 ml PBS, the cell pellets were lysed with chilled cell lysis buffer (Cell Signaling Technology, #9803) supplemented with Halt™ protease inhibitor cocktail (Thermo Scientific, #78430) and phosphatase inhibitor (Sigma-Aldrich, # 4906837001) for 30 min with intermittent vortexing. The lysate was transferred into PCR-strip tubes and sonicated in a chilled water bath sonicator (QSonica). Lysates were clarified by centrifugation at 15,000 rpm at 4 °C for 15 min. Protein concentration was determined using BCA protein assay kit (Pierce, #23225). The lysates were mixed with LDS sample buffer (Life Technologies, NP0008) and sample reducing agent (Life Technologies, NP0009), followed by heating at 70 °C for 10 min to fully denature the protein. The protein extract (20 µg) was separated on 4–12% NuPAGE Bis-Tris gels (Life Technologies WG1403A), followed by transferring onto nitrocellulose membranes using the Trans-Blot® Turbo™ semi-dry system (Bio-Rad). Membrane blots were pre-stained with total protein stain (LI-COR, # 926-11016) and imaged with Odyssey® CLx. The blots were subsequently blocked for 1 h at room temperature with Intercept® (TBS) blocking buffer (LI-COR, # 927-60001). The blots were finally probed, for overnight at 4 °C, with the appropriate primary antibodies diluted in Intercept® (TBS) blocking buffer supplemented with 0.1% (v/v) Tween-20, followed by the secondary antibodies (IRDye® 800CW donkey anti-rabbit or anti-mouse IgG, LI-COR) for 1 h at room temperature. Fluorescent signals were imaged and quantified using Odyssey® CLx and Image Studio v5.0. Primary antibodies used were: STUB1/CHIP (Cell Signaling Technology, #2080, 1:2000 dilution), STAT1 (Cell Signaling Technology, #14995, 1:10,000 dilution), phospho-Tyr701-STAT1 (Cell Signaling Technology, #9167, 1:2,000 dilution), STAT2 (Cell Signaling Technology, #72604, 1:2000 dilution), IRF1 (Cell Signaling Technology, #8478, 1:2000 dilution), PSMB8 (Cell Signaling Technology, #13635, 1:2,000 dilution), PSMB9 (Abcam, ab184172, 1:10,000 dilution), and PSMB10 (Abcam, ab183506, 1:10,000 dilution).

qPCR analysis

Total RNA was extracted from the tumour cells using RNeasy plus mini kit (Qiagen, #74134) according to the manufacturer's instructions. A total of 1 µg RNA was reversely transcribed in a 20 µl reaction mixture using high-capacity cDNA reverse transcription kit (Applied Biosystems, #4368814) according to the manufacturer's instructions. The resulting cDNA mixture was diluted to 100 µl with nuclease-free water and an aliquot of 2 µl was used for each qPCR set-up. The qPCR was conducted with QuantStudio 12K Flex using power SYBR™ green PCR master mix (Applied Biosystems, #4368577) and 500 nM primer set (IDT PrimeTime) in a total volume of 10 µl reaction in 384-well plates. The PCR cycle is as follow: incubation at 95 °C (10 min), followed by 40 cycles of 95 °C (15 sec) and 60 °C (60 sec). Four technical replicates were performed in parallel for each biological replicate. ΔCT was calculated by taking the difference between the mean CT value ($n = 4$) for each gene of interest and the mean CT value ($n = 4$) of a reference gene (gene name: *Tbp*) within a biological sample. Fold change in gene expression was derived from the ΔΔCT using untreated gControl cells as the reference. PCR primer set for

Ifngr1: ATGATCAGAAATGTTGGTGCAG and TTGAACCCTGTCGTATGCTG;

Stat1: GACTTCAGACACAGAAATCAACTC and TTGACAAAGACCACGCCTT;

Irf1: ACTCAGACTGTTCAAAGAGCTTC and GTCACCCATGCCTTCCAC;

Tbp: CCAGAACTGAAAATCAACGCAG and TGTATCTACCGTGAATCTTGGC.

Gene expression profilling with NanoString

CRISPR-engineered B16-F10 cells (gControl, gStub1 #1, and gStub1 #2) were seeded separately in 12-well plate (50,000 cells per well) with DMEM + 10% FBS. After overnight incubation, the culture media were replaced with fresh media (DMEM + 10% FBS) supplemented with 0.03 ng ml^{-1} of recombinant mouse IFNγ (R&D Systems, #485-MI-100). Total RNA from untreated cells (24 h) and IFNγ-treated cells (6 or 24 h) were extracted with RNeasy plus mini kit (Qiagen, 74134) according to manufacturer's protocol. An input of 150 ng RNA from each sample was mixed with the NanoString reporter and capture probes (nCounter Mouse PanCancer IO 360, # XT-CSPS-MIO360-12), and incubated at 65 °C for 20 h. The hybridized samples were processed on the nCounter prep station, and the resulting cartridge was scanned by the nCounter digital analyzer using 555 fields of view. Raw count data were evaluated for quality control and normalized with 19 housekeeping genes using nSolver 4.0 software (Supplementary Table 3). *Tlk2* was excluded from the housekeeping gene due to weak expression (RNA counts <80). Fold change (FC) was calculated by comparing the normalized RNA counts of each sample to that of the untreated gControl cells as the denominator (Supplementary Table 3). Weakly expressed genes, where the normalized RNA counts were consistently less than 80 in all samples, were excluded from fold change analysis, resulting in an evaluable set of 493 out of 750 genes (Supplementary Fig. 3a). As an overview, all 750 targeted genes were included in the scatter plot analysis (Supplementary Fig. 3b–d).

Proteomics by mass spectrometry

CRISPR-engineered B16-F10 cells (gControl, gStub1 #1, and gStub1 #2) were seeded separately in 12-well plate (50,000 cells per well) with DMEM + 10% FBS. After overnight incubation, the culture media were replaced with fresh media (DMEM + 10% FBS) supplemented with 0.03 ng ml^{-1} of recombinant mouse IFNγ (R&D Systems, #485-MI-100). After 24 h treatment, the cells were trypsinized, collected and washed twice with 0.5 ml PBS. The cell pellets collected from three independent experiments on separate day were lysed in 100 µl of lysis buffer containing 4% sodium dodecyl sulfate, 50 mM Tris-HCl pH 7.5, 50 µg ml^{-1} of DNase (Roche, #10104159001), 50 µg ml^{-1} of RNase (Roche, #10109169001) and Halt™ protease inhibitor cocktail (Thermo Scientific, #78430) on ice for 30 min followed by 65 °C for 30 min. Lysates were clarified by centrifugation at 16,000g at 10 °C for 30 min. Protein content was re-extracted from the pellet with 50 µl of lysis buffer, sonicated with a single burst using a probe sonicator and heated at 95 °C for 10 min before centrifugation at 16,000g at 10 °C for 15 min. Lysates from first and second extractions were pooled. Protein concentration was determined using BCA protein assay kit (Pierce, # 23225). Detergent removal and protein digestion were performed in centrifugal suspension trap columns (Protifi, C02-micro) according to the manufacturer's instructions. Briefly, 80 µg protein extract from each sample was reduced with 50 mM

dithiothreitol (Sigma, #43815) at 95 °C for 10 min and then alkylated with 100 mM iodoacetamide (Sigma, I2512) in the dark at ambient temperature for 30 min. The samples were acidified with 1.2% of phosphoric acid and mixed well with washing buffer consisting of 90% methanol and 100 mM ammonium bicarbonate. The samples were transferred to the suspension trap columns and centrifuged at 4000 g for 30 s. The columns were washed 3 times with washing buffer. Proteins trapped in the suspension bed were digested in 50 mM ammonium bicarbonate with trypsin and endoproteinase Lys-C (Promega, V5073) at enzyme to protein ratio 1:25 in a 47 °C waterbath for 2 h. Peptides were eluted firstly with 50 mM ammonium bicarbonate, then with 0.2% formic acid and lastly with 50% acetonitrile and 0.2% formic acid. The eluates were pooled and vacuum dried completely. Dried peptides were reconstituted with 0.1% formic acid in water, followed by injecting 4 µg for mass spectrometry analysis. Peptides were loaded on a reverse phase EASY-Spray^{TM} column (50cm × 75 µm inner diameter) operated using Easy-nLC^{TM} 1200 (Thermo Fisher Scientific) coupled online to a Q-Exactive HF-X mass spectrometer (Thermo Fisher Scientific). Peptides were separated using a 120 min linear gradient at a flow rate of 300 nL min^{-1}. The Q-Exactive was operated in 'top-10' data-dependent acquisition (DDA) mode with full scan acquired at a resolution of 120,000 (scan range 200–1800 m/z) with an automatic gain control (AGC) target of 3e6. The top ten most abundant ions from the full scan were isolated with an isolation width of 0.7 m/z and fragmented by higher energy collisional dissociation (HCD) with normalized collision energy (NCE) of 27. MS/MS scan was acquired at a resolution of 30,000 with an AGC target of 1e5. The default charge state was set at 2 and dynamic exclusion was enabled for 10 s. Maximum ion injection time for full scan and MS/MS scan were 100 ms and 105 ms respectively.

DDA raw files were processed with Proteome Discoverer 2.4 using Sequest HT search engine where mass spectrometric data was searched against SwissProt TaxID 10090 mouse database (v2017-10-25). Percolator was used to validate search results based on the concatenated mode where only the best scoring PSMs (target/decoy) were considered. Trypsin was specified as the enzyme, cleaving after all lysine and arginine residues and allowing up to two missed cleavages. Carbamidomethylation of cysteines was set as fixed modification while variable modifications included oxidation of methionine, acetylation of N-terminus, N-terminal loss of methionine and N-terminal loss of metionine along with the addition of an acetyl group. The minimum peptide length required for protein identification was six amino acids. Precursor and fragment mass tolerances were set as 10 ppm and 0.02 Da respectively. Overall, a total of 3048 proteins were detected by mass spectrometry (n = 6 replicates per cell group, 3 biological replicates × 2 mass spectrometry replicates). After quality control (>1 unique peptide found or 1 unique peptide with ≥ 25% coverage), we obtained a high-quality dataset of 2293 proteins for further differential enrichment analysis (Supplementary Table 4). The adjusted P values were determined by unpaired t test per protein (without assuming a consistent standard deviation) and false discovery rate approach (two-stage step-up method of Benjamini, Krieger, and Yekutieli, with Q = 5%). Differentially expressed proteins are defined by Log_2 (Fold change) >1 and -Log_{10} (adjusted P) >1.301 (Supplementary Table 4).

Isothermal titration calorimetry (ITC)

Recombinant STUB1 protein (aa25-aa153) was dialyzed overnight with Slide-A-Lyzer cassette (7K MWCO, Thermo Scientific, #66373) in 1 liter of dialysis buffer (PBS, pH 7.4, 0.5 mM TCEP). The dialyzed protein solution was centrifuged at 15,000 rpm for 10 min at 4 °C to remove potential precipiates. The protein was diluted to 20 μM using the dialysis buffer, followed by the additon of DMSO spike-in (2% final concentration). The synthetic peptides (10 mM in DMSO) were diluted to 200 μM with the dialysis buffer (2% final DMSO concentration). ITC measurements were performed at 25 °C using a Microcal PEAQ-ITC (Malvern Panalytical Inc). An initial injection of 0.4 μl followed by a total of 39 injections of peptide solution (1 μl, 200 μM) were added at an intervals of 2 min into the protein solution (20 μM) while stirring at 750 rpm. The data point produced by the first injection was discarded prior to curve fitting in order to account for the diffusion effect during the equilibration process. The experimental data were fitted to a non-interacting one-site binding model using the analysis software supplied by Microcal, with ΔH (enthalpy change), K_a (association constant) and N (number of binding sites per monomer) as adjustable parameters. Free energy change (ΔG) and entropy contributions (TΔS) were determined from the standard equation: $\Delta G = \Delta H - T\Delta S = -RT \ln K_a$, where T is the absolute temperature and R = 1.987 cal mol^{-1} K^{-1}.

Thermal shift assay

The SYPRO Orange fluorescent dye (Invitrogen) was used to measure the thermal stability of recombinant STUB1 protein (aa25-aa153). With increasing temperature, binding of the dye molecule to the hydrophobic region of the denatured STUB1 results in an increase in the fluorescence intensity. The midpoint of this transition is termed the T_m. Binding of a ligand, such as peptide, stabilizes the protein and results in a melting temperature shift (ΔT_m), which correlates with the binding affinity of the ligand. The thermal shift assay was conducted in a CFX96™ real-time PCR detection system (Bio-Rad). A total of 50 μl mixture containing 3.125× SYPRO Orange (Invitrogen, diluted from 5000× DMSO stock), 100 μM peptide of interest, and 10 μM protein was prepared in a PCR 8-well strip tube. The samples were heated from 25 to 95 °C in 0.5 °C increment each cycle. The holding time for each cycle is 5 sec, after which the fluorescence intensity was measured in Channel 2 (HEX) with Ex/Em:515−535/560−580 nm. Each independent experiment was performed in technical duplicates.

Competitive fluorescence polarization

The assays were performed at room temperature using assay buffer (PBS, pH 7.4, 0.01% v/v Tween 20) and black 384-well non-binding polystyrene microplate (Greiner Bio-one, #784900). The peptide of interest was first diluted (10-point, 3-fold serial dilution) with the assay buffer on the microplate to have a volume of 10 μl in each well. This was followed by the addition of 10 μl mixture containing 5-FAM-SSGPTIEEVD-CO_2H (30 nM) and the recombinant STUB1 protein (2 μM). The final assay solution (20 μl) contains 5-FAM-labeled tracer peptide (15 nM), protein (1 μM) and peptide of interest (5 nM to 100 μM). After 30 min incubation in the dark, the microplate was read with TECAN Infinite M1000 PRO (Ex: 470 nm, Em: 520 nm, bandwidth: 5 nm, G-factor = 1.05, gain: optimal, #flashes = 10, settle time = 0 ms, z position: calculated from

well). Value of polarization (mP) = 1000 × (G × intensity∥ – intensity⊥) / (G × intensity∥ + intensity⊥). Half maximal inhibitory concentration (IC_{50}) was determined by fitting the curve using 4-parameter sigmoidal function in GraphPad Prism. Each independent experiment was performed in technical triplicates.

Co-immunoprecipitation of FLAG-mCherry2-peptide and STUB1

B16-F10 cells stably expressing the biologic were harvested, rinsed with PBS, and lysed with chilled cell lysis buffer (Cell Signaling Technology, #9803) supplemented with Halt™ protease inhibitor cocktail (Life Technologies, #78430) and phosphatase inhibitor (Sigma-Aldrich, # 4906837001). Cellular lysates were clarified by centrifugation at 15,000 rpm at 4 °C for 15 min. Protein concentration was determined using BCA protein assay kit (Pierce, #23225). For each sample of the co-immunoprecipitation (co-IP), 20 µl of anti-FLAG magnetic beads (Sigma-Aldrich, M8823) was rinsed twice with 0.2 ml PBS, followed by addition of 500 µl diluted cellular lysate (60 µg, 0.12 µg μl^{-1}). For competitive inhibition, synthetic peptide (SIWWPD) was added into the co-IP mixture. The resulting mixture was rotated at room temperature for 4 h, after which the beads were rinsed with 3 × 0.5 ml PBS to remove the unbound proteins. Bound protein complexes were directly eluted with a 20 µl solution of LDS sample buffer (Life Technologies, NP0008) supplemented with sample reducing agent (Life Technologies, NP0009), followed by heating at 70 °C for 10 min. The co-IP final extract was separated on 4–12% Bolt Bis-Tris gels (Life Technologies). Blotting was similar to the Western Blot section described above. Primary antibodies used were: STUB1/CHIP (Cell Signaling Technology, #2080, 1:1000 dilution), FLAG (Sigma-Aldrich, F1804, 1:1000 dilution). As a comparison, 30 µg of whole cell lysates (half amount for the input of co-IP) were loaded along with the co-IP final extract in the gel.

The Cancer Genome Atlas dataset analysis

The Cancer Genome Atlas (TCGA) database was used for analysis of clinical relevance. RNA-sequencing data for 9963 tumors and somatic alterations data for 6384 tumors were obtained through TCGA portal (https://portal.gdc.cancer.gov/) as of September 2015. The expression data were Log10 transformed. Spearman correlation was used to determine the correlation and Wilcoxon rank-sum test was used to calculate *P* value. Statistical analyses and visualizations were performed with Matlab R2010b Version 7.11.2. TMB cutoff for the pan-tumor clinical cohort were the Youden Index value derived in AUROC analysis. An additional, exploratory, pan-tumor TMB threshold was derived by using TMB and GEP data, similar to a previously described method[57].

Statistical analysis

Except for the public RNAseq data, all statistical analyses were performed using GraphPad Prism 8.1.1 (GraphPad) and were described in the Figure caption.

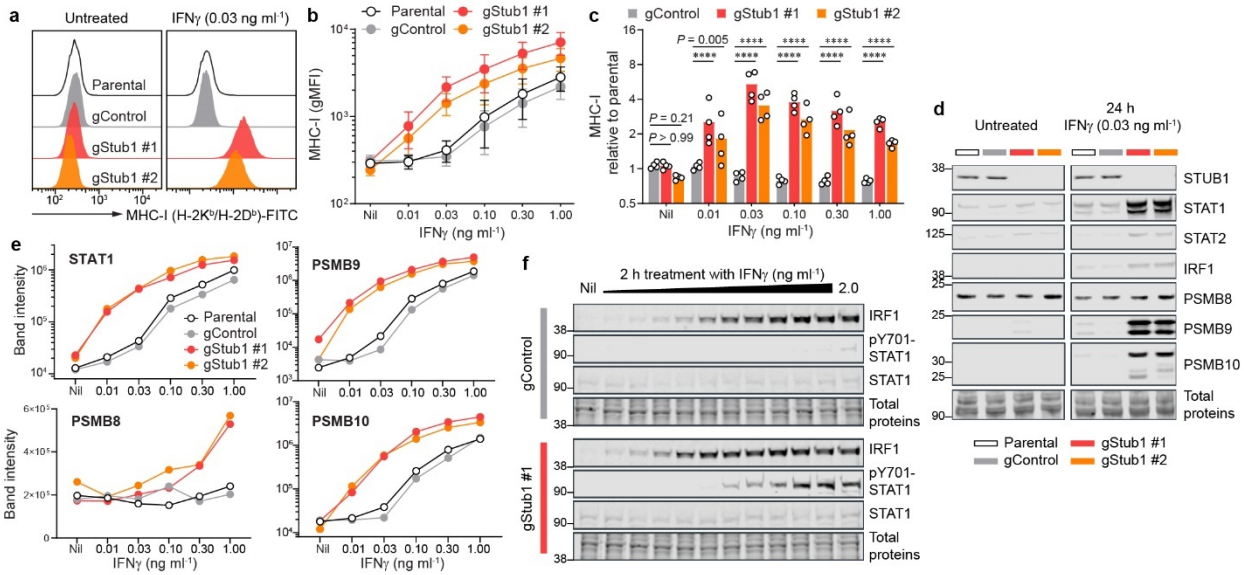

Fig. 1 *Stub1* deletion enhances antigen processing and presentation by sensitizing tumour cells to IFNγ. a–c, Flow cytometry analysis of cell surface MHC-I on parental, control or independent *Stub1*-null B16-F10 cells. gMFI, geometric mean fluorescence intensity. **d**, **e**, Western blot analysis of the expression level of STUB1, STAT1, STAT2, IRF1, PSMB8, PSMB9 and PSMB10 in parental, control or independent *Stub1*-null B16-F10 cells. Band intensity was normalized with total protein signal. The tumour cells were either untreated (Nil) or treated with IFNγ for 24 h (a–e). See Supplementary Fig. 1 for additional flow cytometry plots, Western blot data and analysis (a, d, e). **f**, Western blot analysis of the expression level of IRF1, STAT1, and phosphorylation of Tyr701-STAT1 at 2 h post-treatment with IFNγ (2-fold serial dilution from 2.0 ng ml^{-1}). Representative of four (a) or two (d–f) independent experiments. Data are mean ± s.d. (b) or mean with all data points (c) from four independent experiments. *P* values were determined by ordinary two-way ANOVA on Log2-transformed data with Dunnett's multiple comparisons test, **** $P \leq 0.0001$ (c).

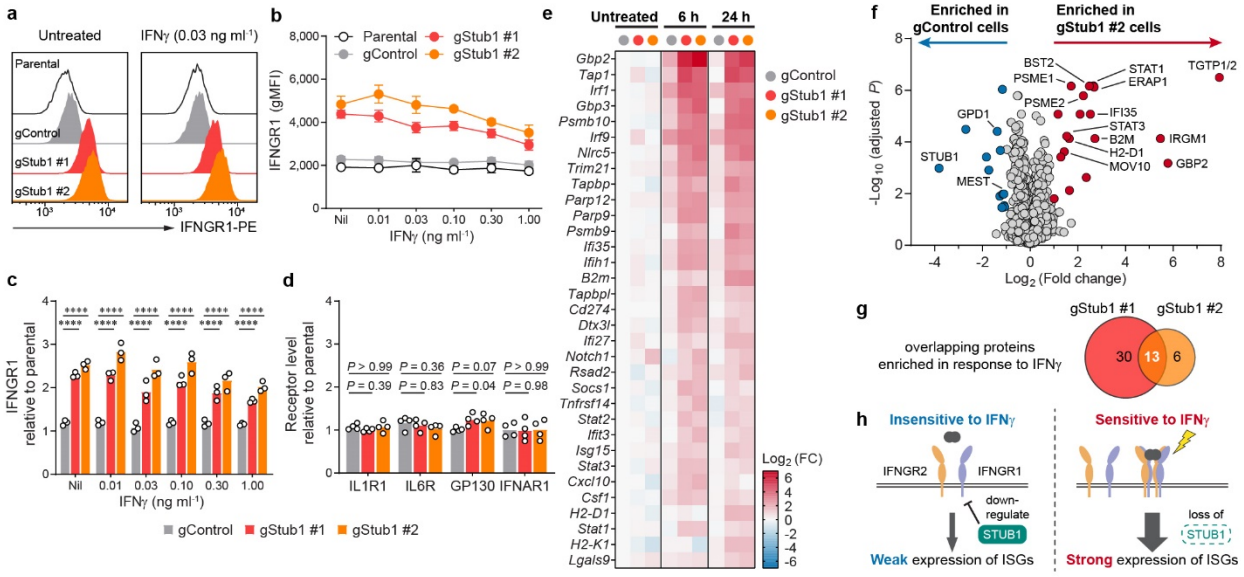

Fig. 2 *Stub1* dampens IFNγ sensing by downregulating IFNGR1. a–c, Flow cytometry analysis of cell surface IFNGR1 on parental, control or independent *Stub1*-null B16-F10 cells which were either untreated (Nil) or treated with IFNγ for 24 h. See Supplementary Fig. 2a for additional plots. **d**, Flow cytometry analysis of the surface level of other cytokine receptors on the tumour cells. See Supplementary Fig. 2b–c for the plots. **e**, Heatmap showing genes (Supplementary Table 3) being upregulated by >2-fold in both gStub1 #1 and #2 cells relative to untreated gControl cells. The cells were treated with 0.03 ng ml^{-1} IFNγ for 6 or 24 h. See Supplementary Fig. 3a for the full heatmap. FC, fold change. **f**, Volcano plot showing differential protein expression in gStub1 #2 versus gControl cells, following stimulation with 0.03 ng ml^{-1} IFNγ for 24 h. Red or blue circles highlight proteins significantly enriched in gStub1 #2 or gControl cells respectively (2-fold cutoff, adjusted $P \leq 0.05$; $n = 6$ replicates per cell group, 3 biological replicates × 2 MS replicates). See Supplementary Fig. 3e for data of gStub1 #1 cell. **g**, MS proteomics uncovered 13 proteins commonly enriched in both gStub1 #1 and #2 cells. The overlapping proteins are explicitly labeled in panel **f**. **h**, Proposed model whereby *Stub1* is an intracellular checkpoint that curbs the tumour cells' ability to sense and respond to IFNγ by downregulating IFNGR1. Representative of three independent experiments (a). Data are mean ± s.d. (b) or mean with all data points (c) from three independent experiments. Data are mean with all data points from four independent experiments (d). *P* values were determined by ordinary two-way ANOVA (c) or one-way ANOVA (d) on Log2-transformed data with Dunnett's multiple comparisons test, **** $P \leq 0.0001$.

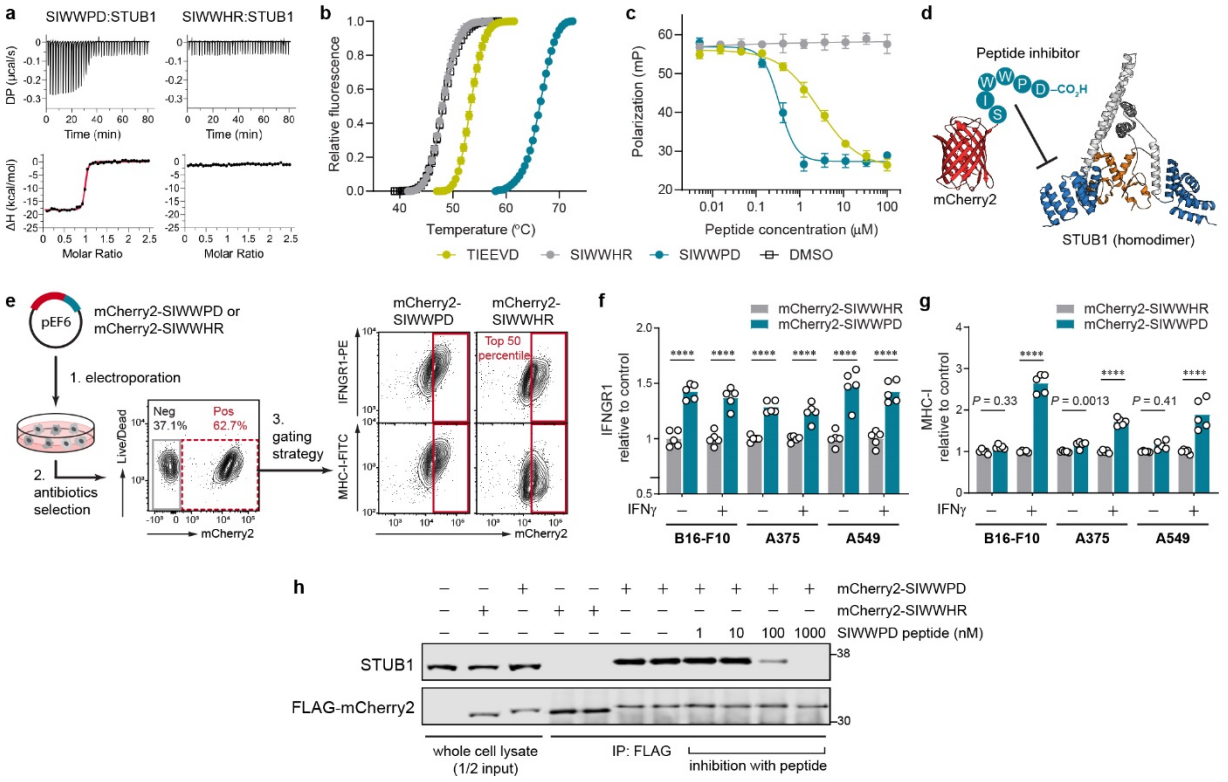

Fig. 3 Pharmacological inhibition of STUB1 with expressed biologic phenocopies the genetic knockout. a, **b**, Validation of the binding of synthetic peptides to STUB1 (aa25–aa153) by isothermal titration calorimetry (a) and thermal shift assay (b). Representative of three independent experiments (a). Data are mean ± s.d. of six replicates derived from three independent experiments (b). **c**, Competitive fluorescence polarization assay. Synthetic peptides were assessed for their ability to compete with 15 nM of tracer peptide (5-FAM-SSGPTIEEVD) for binding to 1 μM STUB1 (aa25–aa153). Data are mean ± s.d. of six replicates derived from two independent experiments. **d**, Design of the inhibitory biologic by grafting the peptide (SIWWPD) to the C-terminus of an mCherry2 (red) scaffold. The fused peptide blocks the function of the tetratricopeptide repeat domain (blue) of STUB1 (PDB code 2C2L) and inhibits its substrate binding. U-box domain (orange) which recruits the E2 ubiquitin-conjugating enzyme is not affected. **e**, Generation of tumour cell lines stably expressing the biologic or its control. Plasmid encoding the biologic was electroporated into tumour cells, followed by antibiotics selection of the stable clones. The mCherry2-positive cells (red dotted box) were further gated for mCherry2^{hi} population (top 50th percentile, red box). Gating example represents IFNγ-treated B16-F10 stable cell lines. **f**, **g**, Flow cytometry analysis of the relative cell surface level of IFNGR1 (f) and MHC-I (g) expressed by the mCherry2^{hi} population in B16-F10, A375 or A549 cells. The cells were either untreated or treated with mouse IFNγ (0.03 ng ml^{-1}) or human IFNγ (0.01 ng ml^{-1}) for 24 h. The expression levels were normalized to the average value of the control (mCherry2-SIWWHR). n = 5 biological replicates from two independent experiments (f–g). Bars are mean with all data points (f–g). P values were determined by ordinary two-way ANOVA in each cell type with Sidak's multiple comparisons

test, **** $P \leq 0.0001$ (f–g). **h**, Co-immunoprecipitation (co-IP) of FLAG-mCherry2-peptide and STUB1 from the cellular lysate of B16-F10 using anti-FLAG antibody. Synthetic peptide (SIWWPD) was added into the co-IP mixture to assess specificity of the interaction. Blot is representative of three independent experiments.

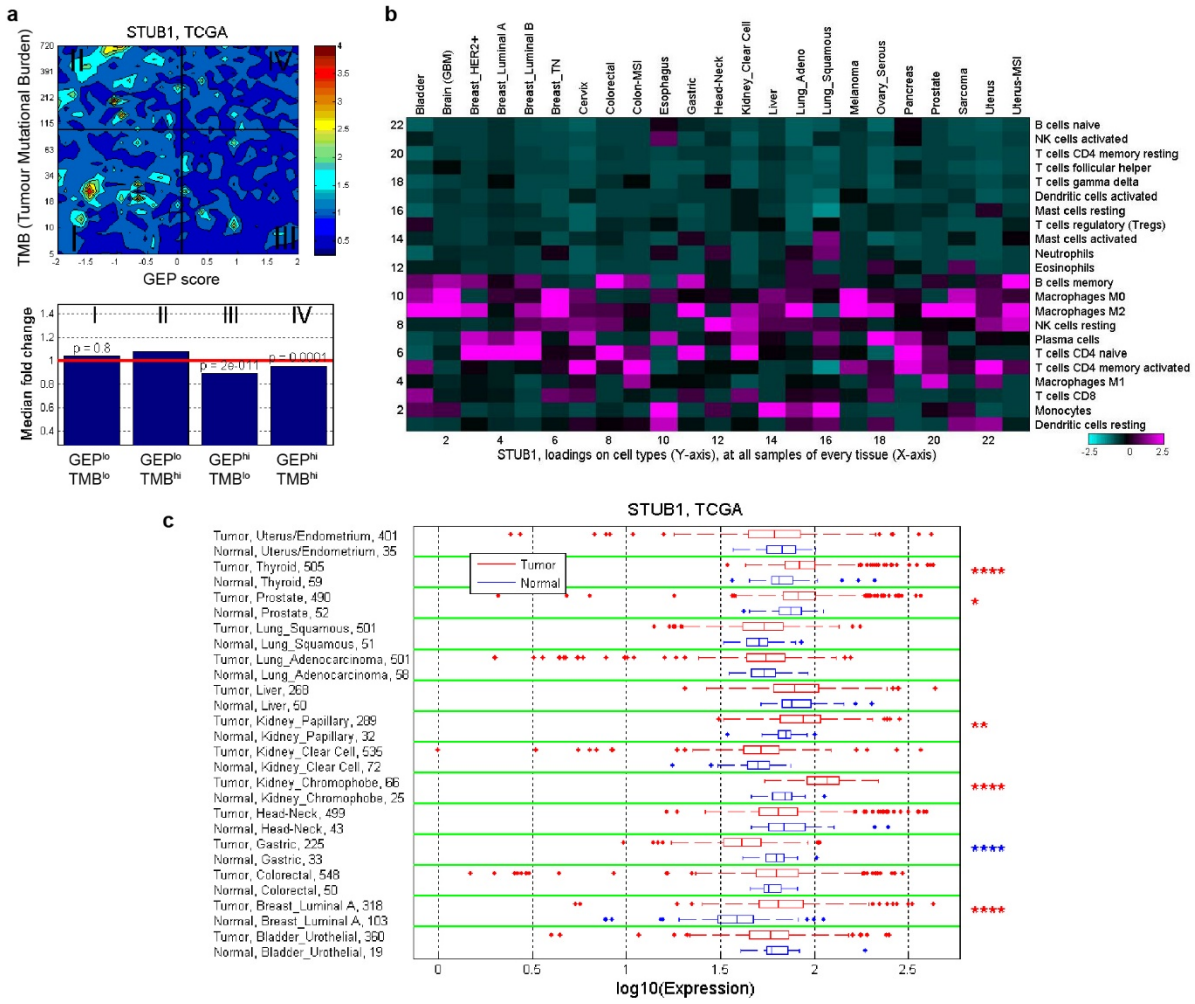

Fig. 4 Correlation and expression of *STUB1* gene in TCGA dataset. a, Contour plot illustrates the association of *STUB1* with TMB and GEP. Blue and red represent under- and overexpression, respectively. TMB cut-off was set at 100 and GEP cut-off corresponds to 55th percentile value for pan-cancer cohort. **b**, *In-silico* deconvolution analysis of bulk RNAseq data from TCGA was used to establish the association between *STUB1* expression and different cell types. Deconvolution analysis was performed separately for each tumor type. **c**, Expression of *STUB1* in tumor tissue and adjacent normal tissue is compared across tumor types for which both tumor and adjacent normal samples are available in TCGA dataset. The significance of the difference is indicated with ∗ $P \leq 0.05$, ∗∗ $P \leq 0.01$, and ∗∗∗∗ $P \leq 0.0001$.

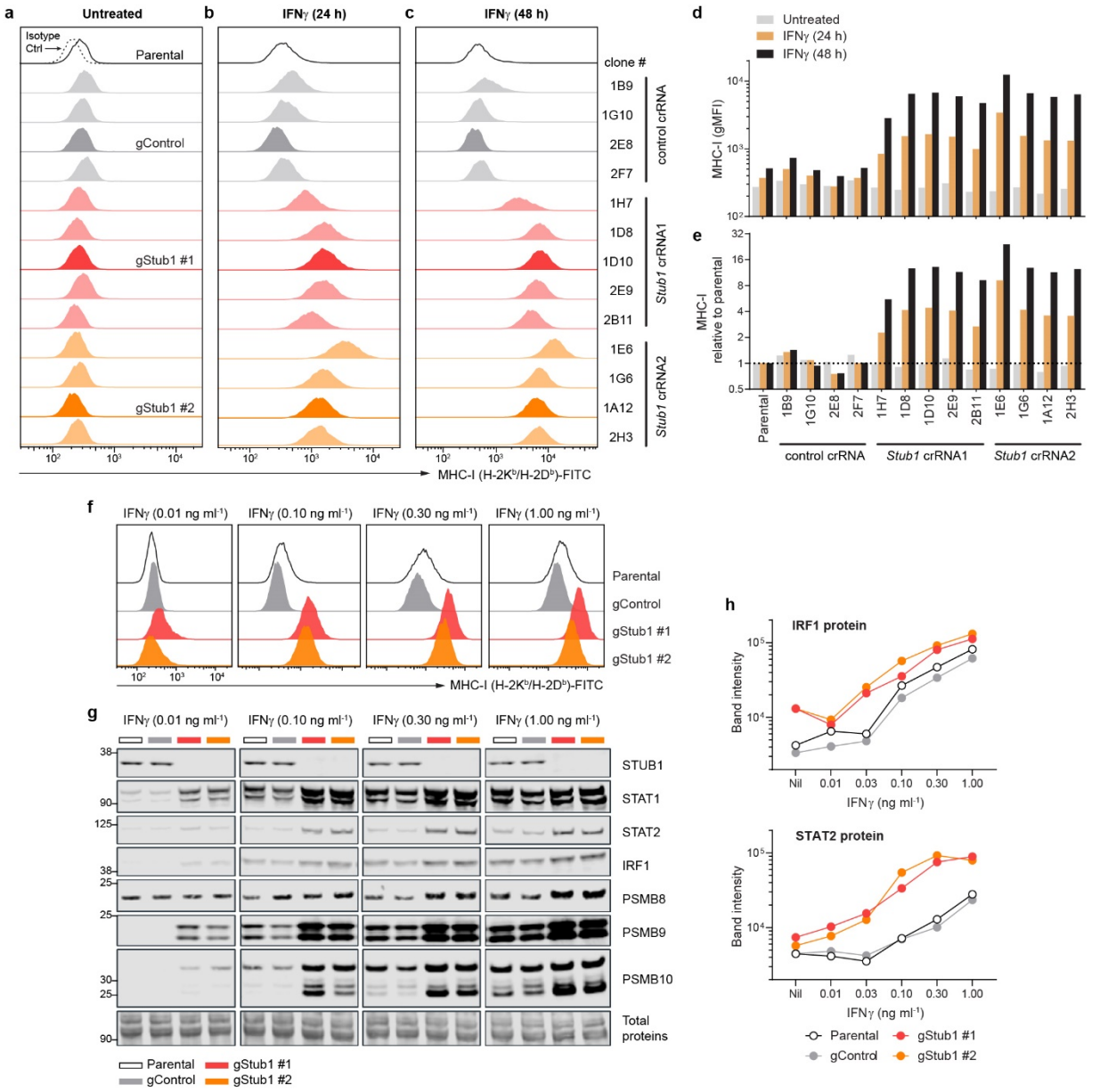

Supplementary Fig. 1 Loss of *Stub1* in B16-F10 melanoma increased the surface level of MHC-I and the protein level of STAT1, STAT2, IRF1, PSMB8, PSMB9 and PSMB10 in response to IFNγ. Related to Fig. 1. **a–e**, Flow cytometry analysis of cell surface level of MHC-I on parental B16-F10 and all CRISPR-edited clones isolated by single-cell subcloning (Supplementary Table 2). The tumour cells were either untreated (a) or treated with 0.10 ng ml^{-1} IFNγ for 24 h (b) or 48 h (c). The expression level of MHC-I on the tumour cells (d) and their relative abundance compared to the parental B16-F10 cells (e). All further experiments were performed using single-cell clone 2E8, 1D10 and 1A12 – termed gControl, gStub1 #1 and gStub1 #2 respectively. **f**, Flow cytometry analysis of cell surface MHC-I on parental, control or independent *Stub1*-null B16-F10 cells, following treatment with the indicated condition for 24 h. **g**, **h**, Western blot analysis of STUB1, STAT1, STAT2, IRF1, PSMB8, PSMB9 and PSMB10 in

tumour cells, following treatment with the indicated concentration of IFNγ for 24 h (g). Quantification of the protein level with LI-COR Image Studio (h). Band intensity was normalized with total protein signal. Representative of four (f) or two (g, h) independent experiments.

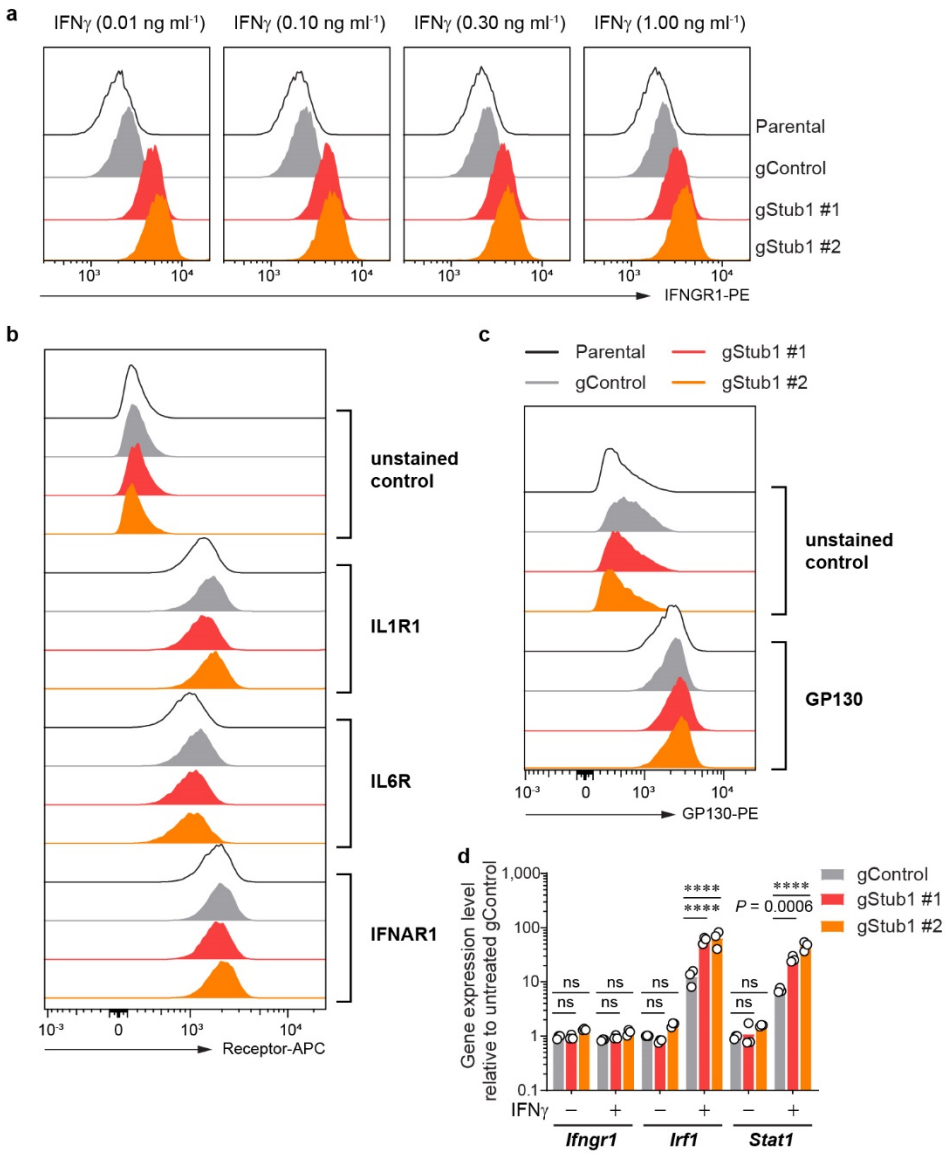

Supplementary Fig. 2 Analysis of the surface level of IFNGR1 and other immune-related receptors, and gene expression of *Ifngr1*, *Irf1* and *Stat1*. Related to Fig. 2. **a**, Flow cytometry analysis of cell surface IFNGR1 on parental, control or independent *Stub1*-null B16-F10 cells treated with IFNγ for 24 h. **b**, **c**, Flow cytometry analysis of cell surface IL1R1, IL6R or IFNAR1 (b) or GP130 (c) on parental, control or independent *Stub1*-null B16-F10 cells at resting state. **d**, qPCR analysis of the gene expression of *Ifngr1*, *Irf1* and *Stat1* relative to untreated gControl cells. Cells were stimulated with IFNγ (0.03 ng ml^{-1}) for 6 h. Expression level was normalized to a reference gene (*Tbp*). Data are mean with all data points from three independent experiments (d). *P* values were determined by ordinary two-way ANOVA in each transcribed gene with Dunnett's multiple comparisons test, **** $P \leq 0.0001$, ns $P > 0.98$ (d). Representative of three (a) or four (b–c) independent experiments.

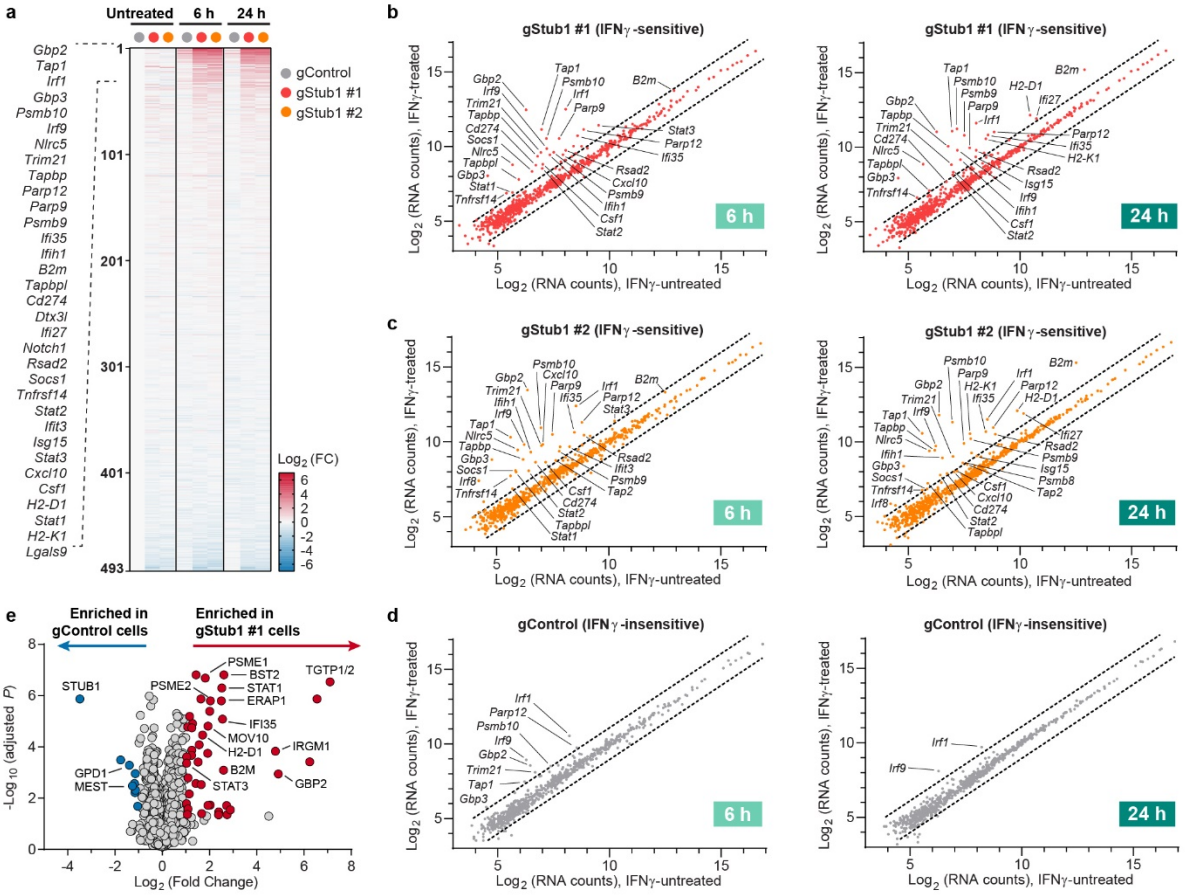

Supplementary Fig. 3 Loss of *Stub1* sensitized B16-F10 melanoma to IFNγ response as determined by gene expression profiling and proteome-wide studies. Related to Fig. 2. **a**, Heatmap showing relative gene expression profile of 493 out of 750 genes (NanoString PanCancer IO 360, Supplementary Table 3) in tumours cells which were either untreated or treated with 0.03 ng ml^{-1} IFNγ for 6 or 24 h. Weakly expressed genes (257 out of 750) were removed from the analysis. 33 genes upregulated by >2-fold in both *Stub1*-null cells relative to untreated gControl cells were listed explicitly (see Fig. 2e for the expanded heatmap). Refer to Method section for the description of fold change analysis. FC, fold change. **b–d**, Scatter plots showing the expression level of all 750 genes (Supplementary Table 3) in gControl cells (b) gStub1 #1 cells (c) or gStub1 #2 cells (d) before and after treatment with 0.03 ng ml^{-1} IFNγ for 6 h (left plot) or 24 h (right plot). Dotted lines depict the boundary of 2-fold change in the RNA counts which were normalized with 19 housekeeping genes. **e**, Volcano plot showing differential protein expression (Supplementary Table 4) in gStub1 #1 versus gControl cells, following treatment with 0.03 ng ml^{-1} IFNγ for 24 h. Red or blue circles highlight proteins being significantly enriched in gStub1 #1 or gControl cells respectively (2-fold cutoff, adjusted $P \leq 0.05$; $n = 6$ replicates per cell group, 3 biological replicates × 2 MS replicates). Enriched proteins that overlap with gStub1 #2 cells (see Fig. 2f–g) are explicitly labeled in the plot. STUB1, GPD1 and MEST were consistently enriched in gControl cells as compared to either

gStub1 #1 or gStub1 #2 cells (see Fig 2f). Statistics detail were described in proteomics method section.

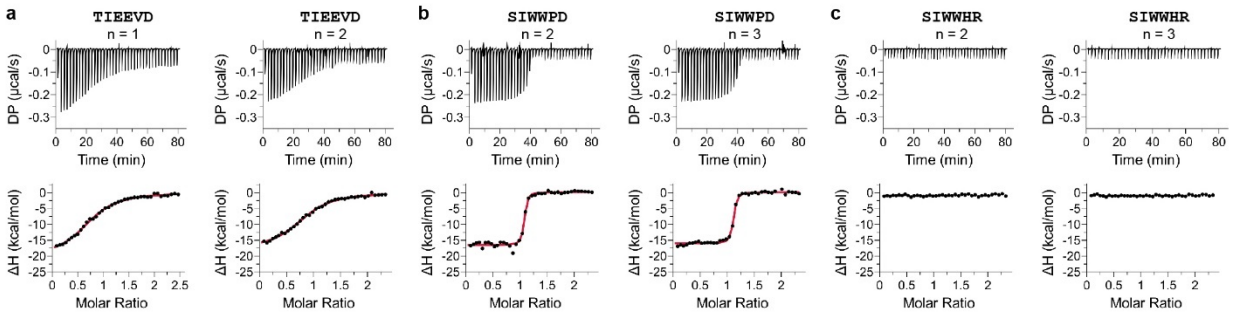

d

	TIEEVD	SIWWPD	SIWWHR
ΔT_m (°C)	5.2 ± 0.2	18.3 ± 0.1	-0.1 ± 0.2
IC_{50} (µM)	2.7 ± 0.2	0.34 ± 0.02	> 100
K_D (nM, ITC)	2190 ± 120	14 ± 2	>10,000
N (ITC)	0.81 ± 0.06	1.03 ± 0.07	NA
ΔH (kcal mol^{-1}, ITC)	-19.3 ± 1.7	-17.1 ± 1.2	NA
$-T\Delta S$ (kcal mol^{-1}, ITC)	11.6 ± 1.8	6.3 ± 1.2	NA

Supplementary Fig. 4 Validation of the binding of synthetic peptides to STUB1 with multiple biophysical assays. Related to Fig. 3. **a**–**c**, Binding of the synthetic peptides to STUB1 (aa25–aa153) as determined by isothermal titration calorimetry (ITC). The peptides contain free carboxylic acid at the C-terminus and are acetylated at the N-terminus. Positive control peptide (TIEEVD) is derived from the C-terminal end of HSPA8 – the endogenous binding substrate of STUB1 (a). SIWWPD bound strongly to the protein (b), whereas, SIWWHR is a non-binding control (c). **d**, Summarized results from all biophysical assays. The shift in the melting temperature (ΔT_m) relative to the DMSO vehicle is reported as mean ± s.d. from three independent experiments. Half maximal inhibitory concentration (IC_{50}) is reported as mean ± s.e. derived from the 4-parameter sigmoidal curve fitted with the data of six replicates derived from two independent fluorescence polarization experiments. Dissociation constant (K_D), binding stoichiometry (N), enthalpy (ΔH) and entropy ($-T\Delta S$) are reported as mean ± s.d. from two (a) or three (b–c) independent ITC experiments.

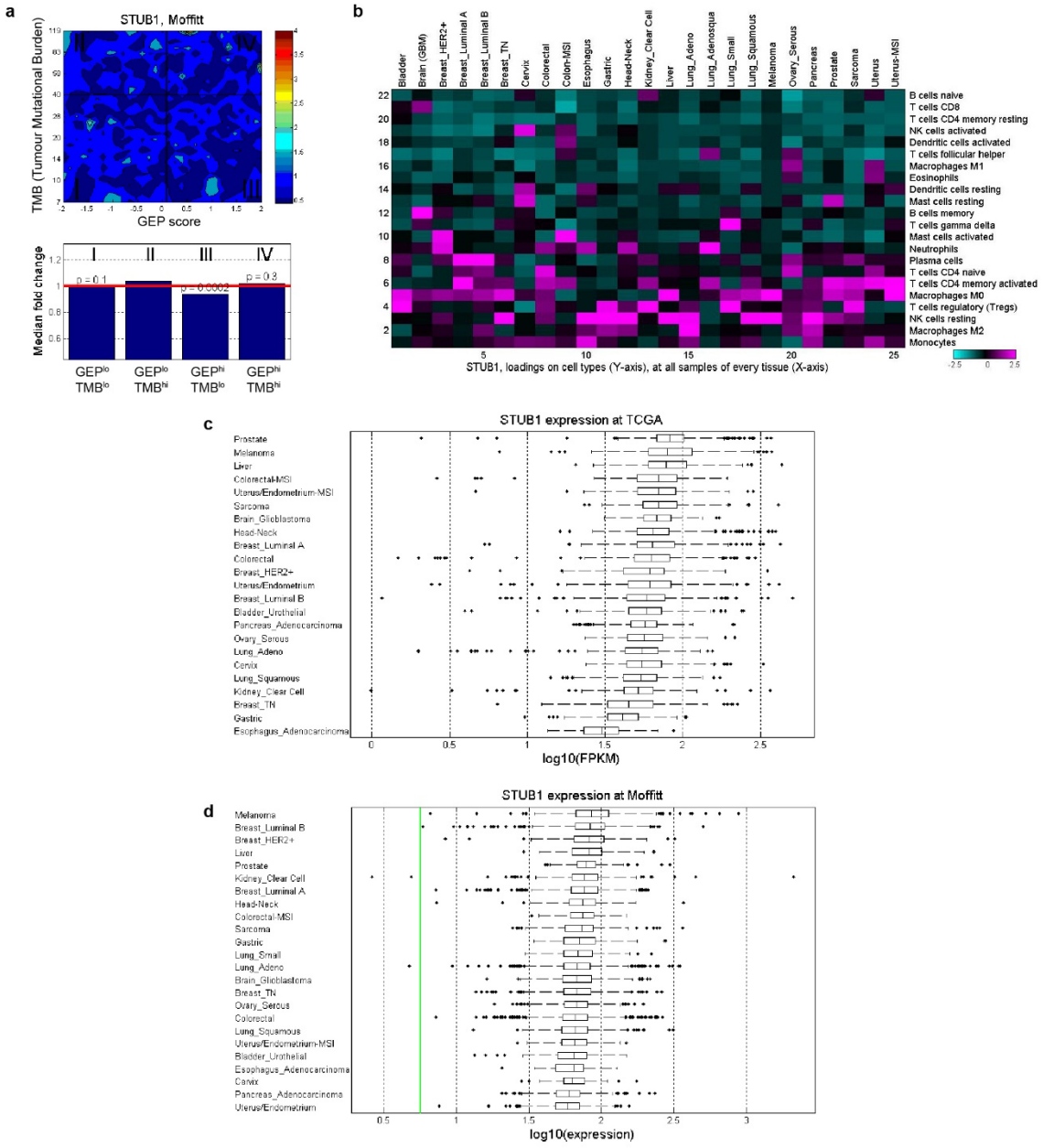

Supplementary Fig. 5 Correlation and expression of *STUB1* gene in Moffitt dataset. Related to Fig. 4. **a**, Contour plot illustrates the association of *STUB1* with TMB and GEP. Blue and red represent under- and overexpression, respectively. TMB cut-off was set at 40 and GEP cut-off corresponds to 55th percentile value for pan-cancer cohort. **b**, *In-silico* deconvolution analysis of bulk RNAseq data from Moffitt was used to establish the association between *STUB1* expression and different cell types. Deconvolution analysis, based on CIBERSORT, was performed separately for each tumor type. **c**, **d**, Relative *STUB1* expression level across major tumour tissues in TCGA (c) and Moffitt (d). Limit of detection >$\log_{10}(-1.7)$ in TCGA. Green line depicts the limit of detection (d).